Low dose tomographic fluoroscopy: 4D intervention guidance with running prior

Barbara Flach,[a] Jan Kuntz, and Marcus Brehm
Medical Physics in Radiology, German Cancer Research Center (DKFZ), Im Neuenheimer Feld 280, 69120 Heidelberg, Germany and Institute of Medical Physics, Friedrich–Alexander–University (FAU) of Erlangen–Nürnberg, Henkestraße 91, 91052 Erlangen, Germany

Rolf Kueres
Medical Physics in Radiology, German Cancer Research Center (DKFZ), Im Neuenheimer Feld 280, 69120 Heidelberg, Germany

Sönke Bartling
Medical Physics in Radiology, German Cancer Research Center (DKFZ), Im Neuenheimer Feld 280, 69120 Heidelberg, Germany and Institute for Clinical Radiology and Nuclear Medicine, University Medical Center Mannheim, Theodor–Kutzer–Ufer 1–3, 68167 Mannheim, Germany

Marc Kachelrieß
Medical Physics in Radiology, German Cancer Research Center (DKFZ), Im Neuenheimer Feld 280, 69120 Heidelberg, Germany and Institute of Medical Physics, Friedrich–Alexander–University (FAU) of Erlangen–Nürnberg, Henkestraße 91, 91052 Erlangen, Germany

(Received 28 March 2013; revised 21 June 2013; accepted for publication 11 August 2013; published 13 September 2013)

Purpose: Today's standard imaging technique in interventional radiology is the single- or biplane x-ray fluoroscopy which delivers 2D projection images as a function of time (2D+T). This state-of-the-art technology, however, suffers from its projective nature and is limited by the superposition of the patient's anatomy. Temporally resolved tomographic volumes (3D+T) would significantly improve the visualization of complex structures. A continuous tomographic data acquisition, if carried out with today's technology, would yield an excessive patient dose. Recently the authors proposed a method that enables tomographic fluoroscopy at the same dose level as projective fluoroscopy which means that if scanning time of an intervention guided by projective fluoroscopy is the same as that of an intervention guided by tomographic fluoroscopy, almost the same dose is administered to the patient. The purpose of this work is to extend authors' previous work and allow for patient motion during the intervention.
Methods: The authors propose the running prior technique for adaptation of a prior image. This adaptation is realized by a combination of registration and projection replacement. In a first step the prior is deformed to the current position via affine and deformable registration. Then the information from outdated projections is replaced by newly acquired projections using forward and backprojection steps. The thus adapted volume is the running prior. The proposed method is validated by simulated as well as measured data. To investigate motion during intervention a moving head phantom was simulated. Real *in vivo* data of a pig are acquired by a prototype CT system consisting of a flat detector and a continuously rotating clinical gantry.
Results: With the running prior technique it is possible to correct for motion without additional dose. For an application in intervention guidance both steps of the running prior technique, registration and replacement, are necessary. Reconstructed volumes based on the running prior show high image quality without introducing new artifacts and the interventional materials are displayed at the correct position.
Conclusions: The running prior improves the robustness of low dose 3D+T intervention guidance toward intended or unintended patient motion. © *2013 American Association of Physicists in Medicine*. [http://dx.doi.org/10.1118/1.4819826]

Key words: computed tomography (CT), flat detector CT, interventional radiology, undersampled reconstructions, minimally–invasive interventions

1. INTRODUCTION

In recent years minimally-invasive interventions like stenting, aneurysm coiling, and biopsies became more and more important because of a quicker recovery of the patient and a reduced risk of infections.[1–3] Since the line of sight is interrupted, the interventional materials used in these procedures, e.g., guide wires and stents are tracked by imaging techniques, for example, by x-ray imaging. Today's state-of-the-art technique in interventional radiology is the single- or

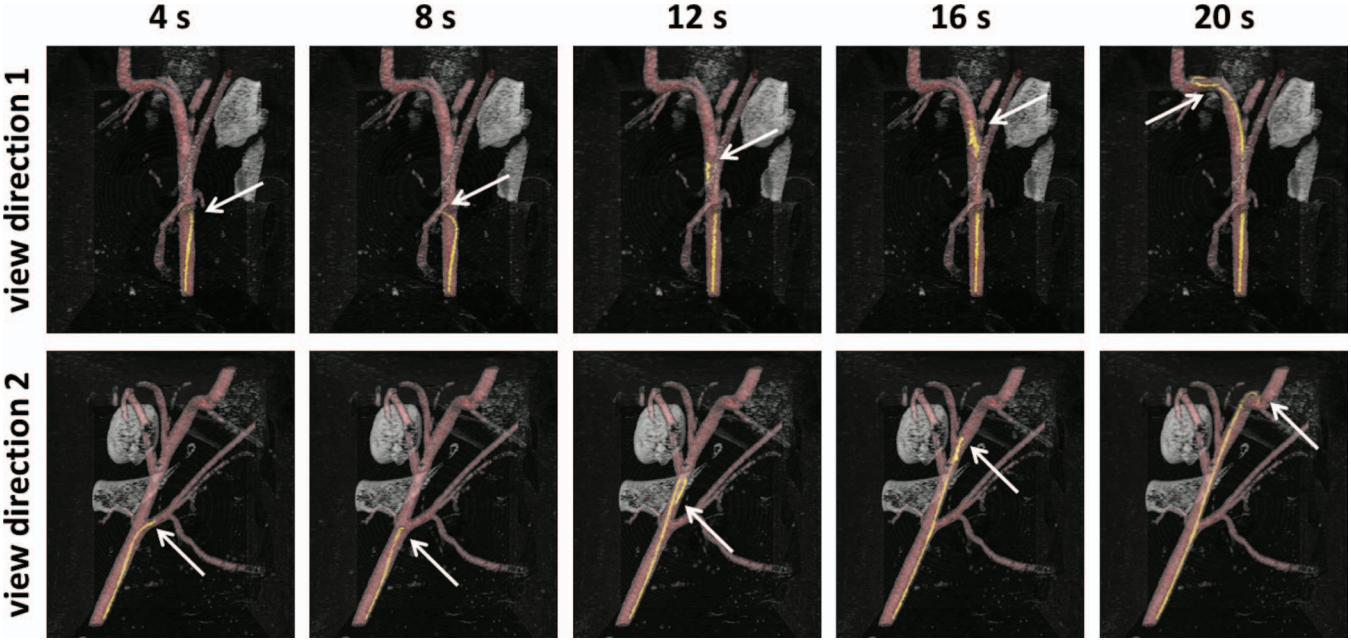

FIG. 1. Several frames of a 4D volume rendering belonging to an intervention where a guide wire is inserted into the carotid of a pig.

biplane fluoroscopy,[4,5] providing two-dimensional images as a function of time (2D+T). We will here refer to this modality as projective fluoroscopy, as opposed to tomographic fluoroscopy that provides three-dimensional images as a function of time (3D+T) and that is the focus of this work.

The downside of projective fluoroscopy is that the images show only a superposition of the patient's anatomy and therefore the visualization of more complex structures and their spatial relationship is difficult and often ambiguous. Nondirected probing, e.g., to guide a wire through the vasculature, is the consequence. This prolongs procedure time and increases radiation dose to the patient as well as to the interventionalist. More directed probing would in addition reduce the trauma to the vasculature.

A continuous display of 3D volumes would significantly improve visualization.[6–8] Especially the position of implanted foreign bodies such as coils and stents would be more clear and therefore the interventions could be safer. However, continuously acquiring CT images for several minutes will typically yield very high patient dose values of 2.3 to 10.4 mGy/s.[9,10] In contrast, dose values of projective fluoroscopy are more than ten times lower.[11] Thus CT fluoroscopy was not able to establish in clinical practice although it is possible with today's technical equipment.[12,13]

For a wide acceptance of tomographic fluoroscopy, the x-ray dose has to be kept as low as in projective fluoroscopy. This means that the volumes need to be reconstructed from an extremely low number of projections acquired at a very low dose level. Our prior, but yet preliminary, work indicated that in case of no patient motion about 10 to 20 projections are sufficient to generate 3D volumes showing the temporally resolved interventional materials at high image quality although acquired at dose levels comparable to projective fluoroscopy.[14,15] To achieve these results a dedicated reconstruction algorithm which is explained in detail in Sec. 2.B was designed that makes extensive use of prior knowledge. This prior knowledge were data reconstructed from an interventional flat detector CT scan with many projections immediately prior to the intervention. The tomographic fluoroscopy data were acquired with the same flat detector CT.

An example for an intervention guided by our low dose tomographic fluoroscopy method is shown in Fig. 1. In this case, a guide wire was inserted into the carotid of a pig *in vivo*. The temporally resolved volumes are reconstructed by the just mentioned algorithm based on a high quality prior image showing the anatomy of the pig and the undersampled intervention scan to determine the current position of the guide wire. The volume renderings, created with the software ImageVis3D,[16] show the pig's anatomy in gray, the vasculature (reconstructed from a contrast-enhanced scan) in red, and the interventional material (the guide wire) in yellow. The volume renderings belong to different points in time and thus

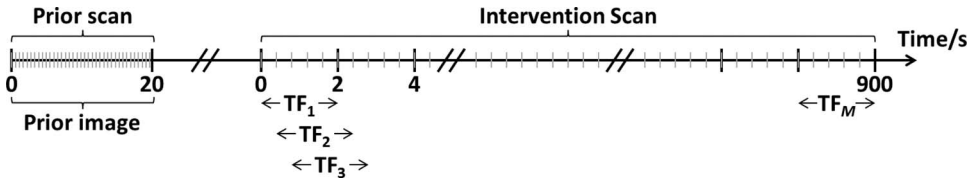

FIG. 2. Potential imaging workflow during an intervention. The vertical tick marks indicate whether the angular sampling is dense or sparse. Apart from the prior scan the workflow is identical to projective fluoroscopy. In contrast to projective fluoroscopy each projection is taken from a different view angle here.

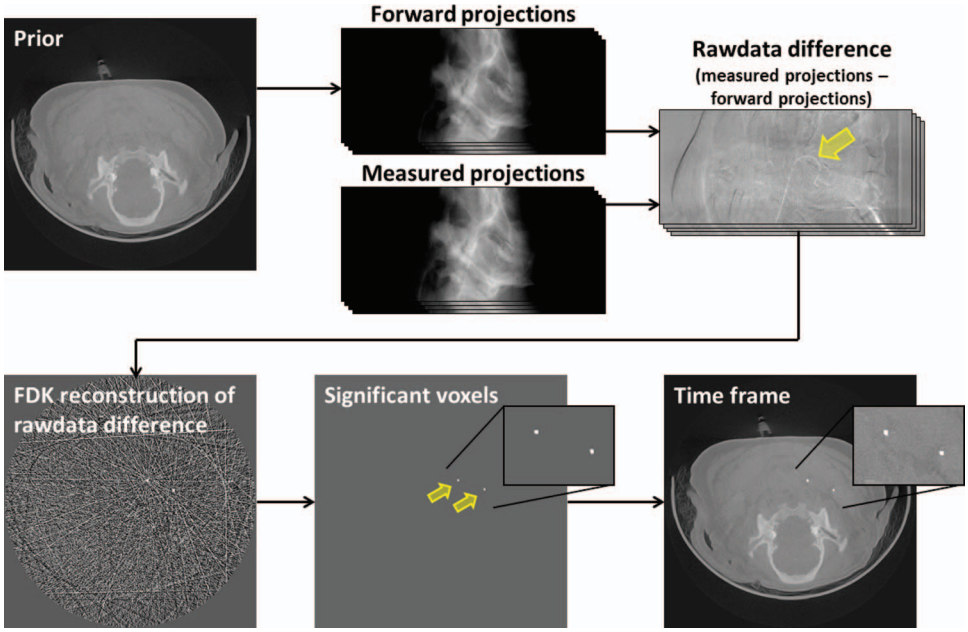

FIG. 3. Illustration of the PrIDICT algorithm. The arrows point to the interventional materials.

show the guide wire at different positions. Similar results (not shown here) were obtained when observing the expansion of a stent.

Other algorithms developed for undersampled data like the ASD-POCS algorithm[17] or the improved total variation (iTV) algorithm,[18] not relying on prior knowledge, are not able to provide volumes of sufficient quality from this highly undersampled data. Alternatives based on prior images like the PICCS algorithm[19] or the volume-of-change (VOC) reconstruction[20] use a smoothness constraint to reduce streak artifacts and noise. They have turned out not to be suitable in the case of intervention guidance because the interventional materials are very small structures (e.g., guide wires and stents).[14,15]

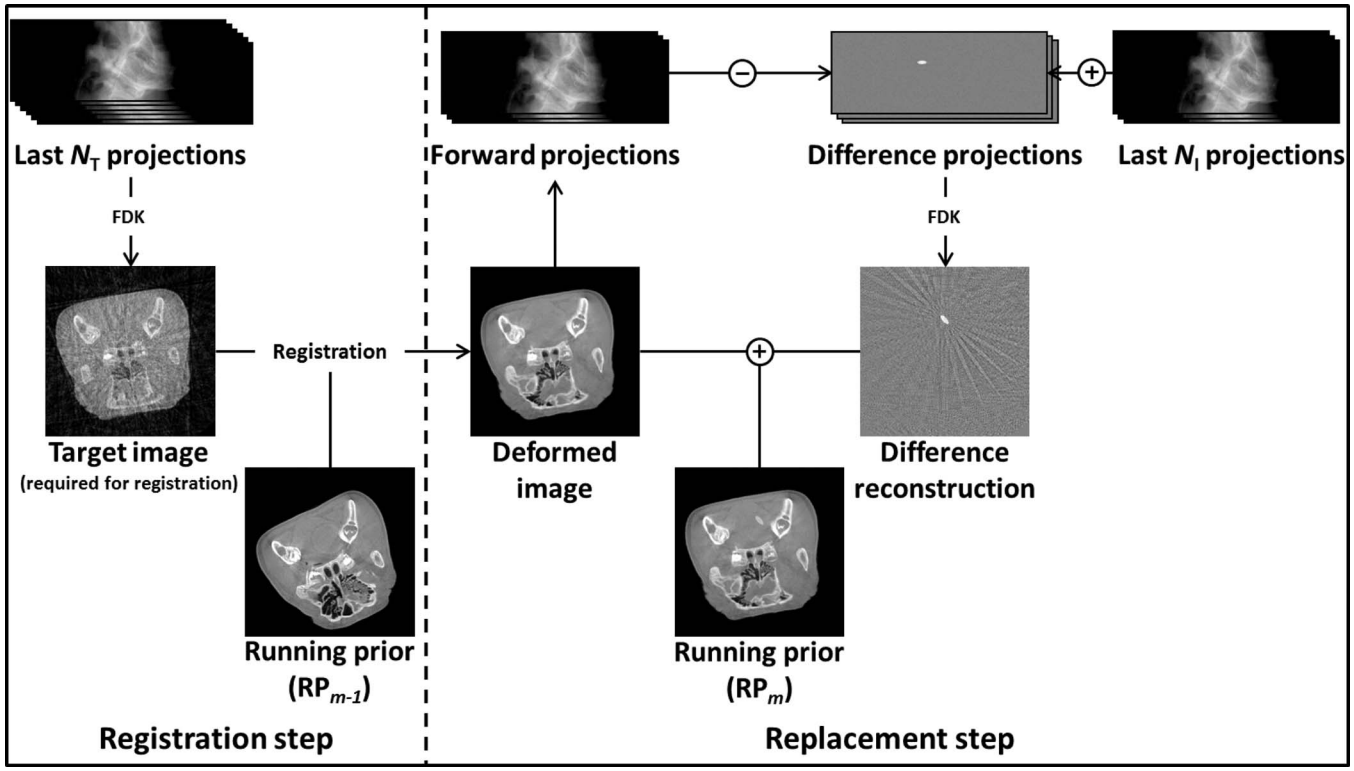

FIG. 4. Illustration of the running prior algorithm.

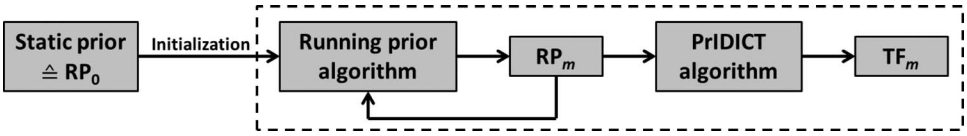

FIG. 5. Illustration of the process to adapt the prior knowledge and calculate a time frame.

A disadvantage of using prior knowledge acquired before the intervention is that this information can be early out-of-date, e.g., if the patient moves either during the intervention or between the prior and the intervention scan. To avoid additional dose for acquiring a new prior image the prior knowledge has to be continuously adapted to the patient's position and appearance. For this adaptation, we propose the running prior technique. For each time step of the intervention it provides an up-to-date prior image that is based solely on already acquired projections of the intervention scan and that does not require any additional projections. Consequently no additional dose is administered for the reconstruction of the adapted prior. The temporal resolution of this adapted prior should be as high as possible on the one hand while the image quality should be the same as for the densely sampled initial prior on the other hand.

2. MATERIALS AND METHODS

2.A. Workflow of tomographic fluoroscopy

To realize low dose tomographic fluoroscopy, with low dose referring to dose levels as low as in projective fluoroscopy, the number of projections acquired per second as well as the dose per projection have to be reduced to a minimum. Despite of this minimal information a high temporal resolution is desired and thus an algorithm dealing with strong angular undersampling combined with noisy projections is required. We were able to show that such a low dose dataset consisting of only 10 to 20 projections per time step is sufficient to reconstruct volumes of high image quality reliably showing the current position of the interventional materials in relation to the surrounding tissue.[15] The dose rate for such an intervention scan, which we measured using an extended CTDI-phantom, is about 7.8 mGy/min. This is in the range of today's fluoroscopy with skin entrance dose rates from "less than 1 mGy/min up to several Gy/min."[21] Clinical studies state dose rates from 5 mGy/min up to 90 mGy/min.[22–38]

We call the reconstructed volumes time frames, and denote a specific time frame as TF_m with $1 \leq m \leq M$ and M being the total number of time steps during the whole intervention. The high image quality of the time frames is achieved by using a prior volume acquired before intervention. This is indicated in Fig. 2 illustrating the workflow for an intervention guided by tomographic fluoroscopy.

First, the prior scan acquires angularly well-sampled data. Their reconstruction yields the high quality prior image. The prior scan corresponds to a total dose of about 10 mGy. This dose has to be considered in addition to the dose administered during the intervention scan. Note that this prior scan does not necessarily mean a higher dose compared to today's projective fluoroscopy because many guided interventions today are interrupted from time to time to conduct a tomographic scan that clarifies ambiguous situations.[39–42] The information about the vasculature (roadmap) can be obtained from another scan that is contrast-enhanced. This is how we achieved to show the vessels in Fig. 1. Potentially, this roadmap can also be acquired during the subsequent intervention scan at no additional dose. This, however, has not yet been under investigation.

After the prior scan has been acquired the intervention process starts. Whenever the interventionalist activates the foot switch continuous scanning with only very few projections per second is performed. Based on the projections of the intervention scan the time frames are reconstructed in a temporally overlapping manner. They show the current position of the interventional materials in relation to the patient's anatomy and, if available, in relation to the vasculature with very high temporal resolution.

2.B. Reconstruction using prior data

The data during the intervention scan are acquired with high angular undersampling. Only $N_I \in \{10, \ldots, 20\}$ projections per 180° are used for the reconstruction of each time frame. Time frames can be reconstructed in an overlapping manner such that up to 20 time frames can be provided per 180°. High image quality of the time frames is achieved by using the prior image dynamic interventional computed tomography (PrIDICT) algorithm of Ref. 15 for image reconstruction. PrIDICT assumes that the patient does not move during the intervention and thus the prior and the update images are always perfectly registered.

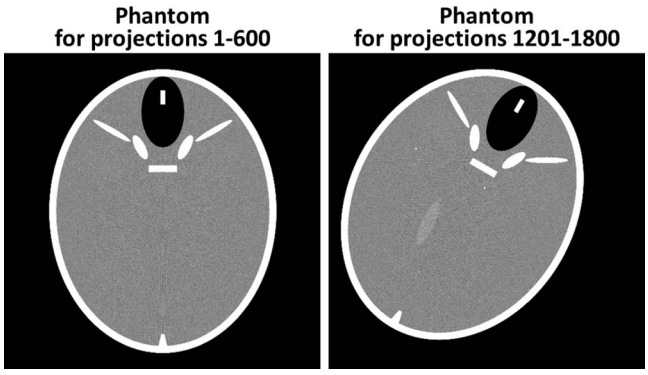

FIG. 6. Phantom used in the simulation study. The images are shown at a gray scale window $C = 0$ HU, $W = 2000$ HU.

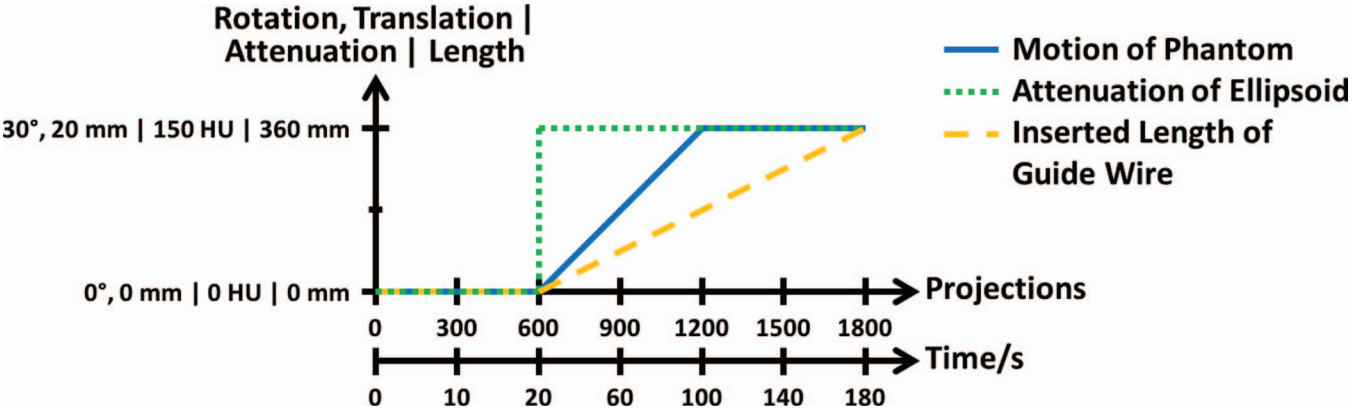

FIG. 7. Motion of the phantom throughout the projections. A time line is shown for comparison with real measurements.

The workflow of the PrIDICT algorithm is illustrated in Fig. 3. N_P projections per 360° are available from the prior scan to reconstruct the prior using the Feldkamp-Davis-Kress (FDK) algorithm.[43] The difference of the forward-projected prior and the N_I latest projections is calculated. These difference projections only show the interventional materials and some noise. FDK is used to reconstruct the difference projections to obtain a volume. This volume is highly deteriorated by streak artifacts, metal artifacts, and noise. Using the knowledge that interventional materials are high contrast objects the L_0-norm is minimized by setting all insignificant voxels to zero. Insignificant voxels are those with a low absolute attenuation in the difference reconstruction. In doing so most of the artifacts are removed. The image containing only the significant voxels is added to the prior image and displayed. Each of these time frames shows the position of the interventional materials in relation to the patient's anatomy and in relation to the roadmap (Fig. 1).

2.C. Motion correction via running prior

The PrIDICT algorithm works well while the patient does not move. But if the patient's position changes between the prior and the intervention scan or even during the intervention itself, so far a new prior is necessary.

FIG. 8. Experimental setup with prototype volume CT and pig *in vivo* and the guide wire within the catheter used for the intervention.

To avoid rescanning the prior, and thus interrupting the intervention, we propose to adapt the prior continuously to the current situation.[44] For each time step $m \in \{1,\ldots,M\}$ the prior of time step $m-1$ is modified to get the prior of time step m. We call those priors the running priors and denote them as RP_m. RP_0 refers to the prior acquired before intervention. We will refer to RP_0 also as the static prior, in particular because the running priors are compared thereto. It should be noted that the extra scan for the static prior could, potentially, also be integrated into the intervention scan itself, e.g., by reconstructing the first N_P projections of the intervention scan.

The adaptation required to convert RP_{m-1} into RP_m is illustrated in Fig. 4. It is a combination of two concepts: deformation via registration (left-hand side of Fig. 4) and substitution of projections with newly measured projection data (right-hand side of Fig. 4). We will detail these steps in the following.

2.C.1. Registration step

For the registration a target image is reconstructed using FDK and the last $N_T \geq N_I$ projections of the intervention scan (top left of Fig. 4). For the results presented here $N_T = 60$ was chosen. The target image represents the current position and appearance of the patient at this time step of the intervention. First an affine registration is applied to estimate the translation (t_x, t_y, t_z) and rotation (r_x, r_y, r_z) between RP_{m-1} and the target image of time step m. For this the mutual information[45] between the two volumes is maximized for example by using an adaptive genetic algorithm[46] or a gradient descent method out of the Insight Toolkit.[48] The result of the affine registration is subsequently refined by applying the demons algorithm[47] to correct for non-rigid motion. The demons algorithm is an intensity-based deformable registration algorithm which calculates voxel-based forces on the assumption of intensity conservation. To ensure a smooth motion estimation the algorithm includes regularization components. The resulting motion vector fields are applied to RP_{m-1} such that the resulting deformed image is well registered with the patient's current density distribution. Thus the registration step corrects for patient motion.

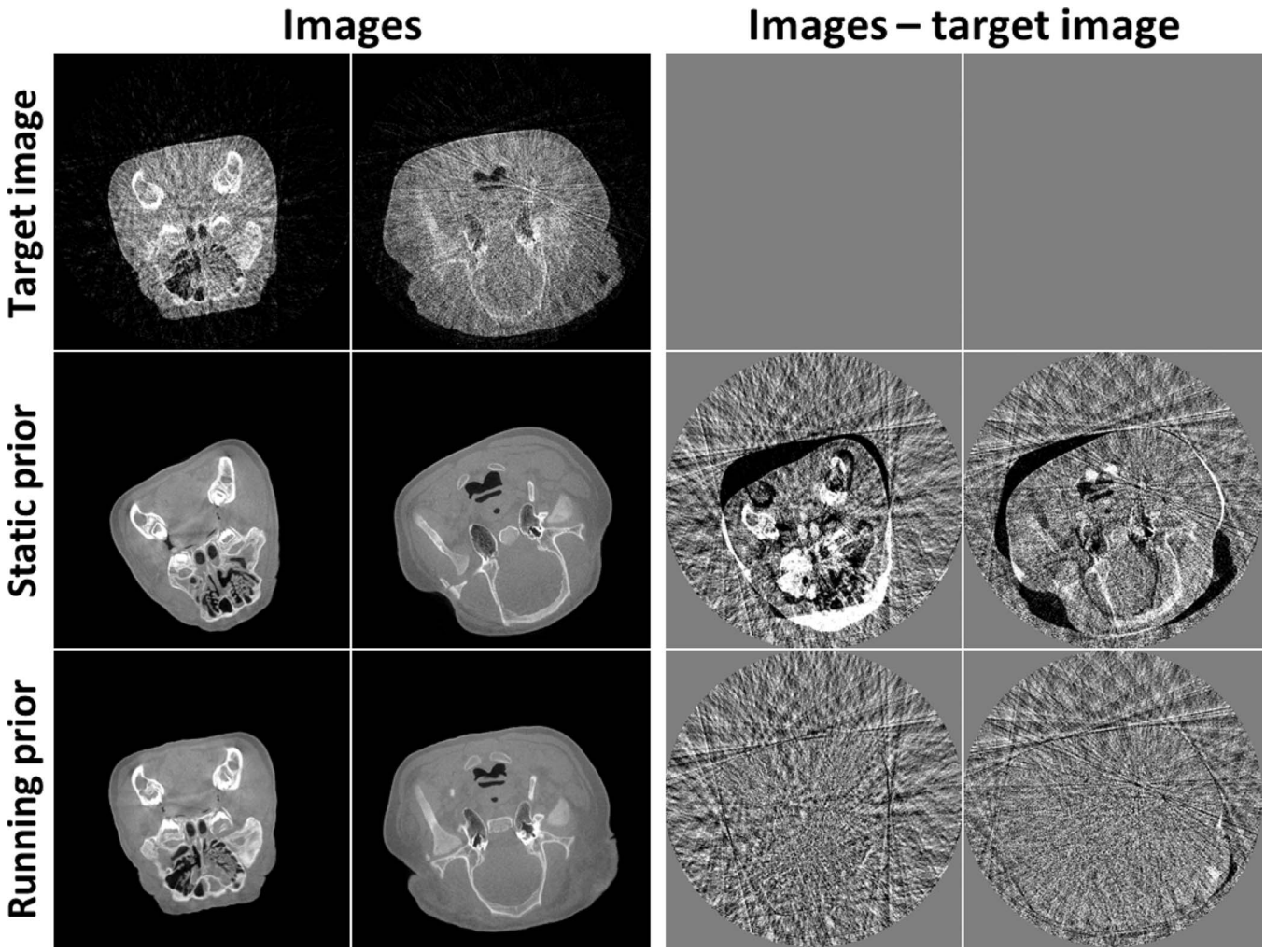

FIG. 9. Left: Position of the pig during the prior scan (static prior) as well as during the intervention scan (target image) and the running prior. The images are shown at a gray scale window $C = 0$ HU, $W = 1500$ HU. Right: Difference images to demonstrate motion between prior and intervention scan and the motion correction by the running prior technique. The images are shown at a gray scale window $C = 0$ HU, $W = 1000$ HU. In each case two slices of the volume are shown.

2.C.2. Replacement step

Furthermore it is necessary that changes in soft tissue, e.g., bleedings that may occur during the intervention, are accounted for by the running prior. To account for such changes the N_I newly measured projections for this time step are used to replace the same number of older projections of the running prior. This is done by forward projecting the deformed image along the geometry of the newly measured projections, by subtracting those forward projection images from the latest measured projection images and by adding the reconstruction of these difference data weighted by the factor $N_\mathrm{I}/N_\mathrm{P}$ to the deformed image. This is our running prior.

2.D. Combining PrIDICT and running prior

The adaptation of the running prior from RP_{m-1} to RP_m is done for each time step $m \in \{1, \ldots, M\}$ during the whole intervention. At each time step the PrIDICT algorithm is applied with RP_m as prior to calculate TF_m for display. In addition RP_m serves as a start image of the running prior algorithm for the calculation of RP_{m+1}. As already mentioned the static prior is used in the first time step for the calculation of RP_1. This process is illustrated in Fig. 5.

2.E. Simulation and measurements

To evaluate the proposed running prior technique in case of motion, we use simulated as well as measured data. The scan geometry is the same for the simulation and the measurement. The distance between focal spot and isocenter is $R_\mathrm{F} = 575$ mm. The distance between detector and isocenter is $R_\mathrm{D} = 355$ mm. The data are acquired using a flat detector with 1024×768 pixels of size $0.388\ \mathrm{mm} \times 0.388\ \mathrm{mm}$. In our study, we use $N_\mathrm{P} = 600$, $N_\mathrm{T} = 60$, and $N_\mathrm{I} = 15$ projections, which means that the prior is reconstructed from 600 projections, the target image for the registration is reconstructed from 60 projections while the reconstruction of the interventional materials in the time frames requires only 15 projections. Consequently, the temporal resolution of the target image is four times lower than the temporal resolution of the interventional materials in the time frames. The images are

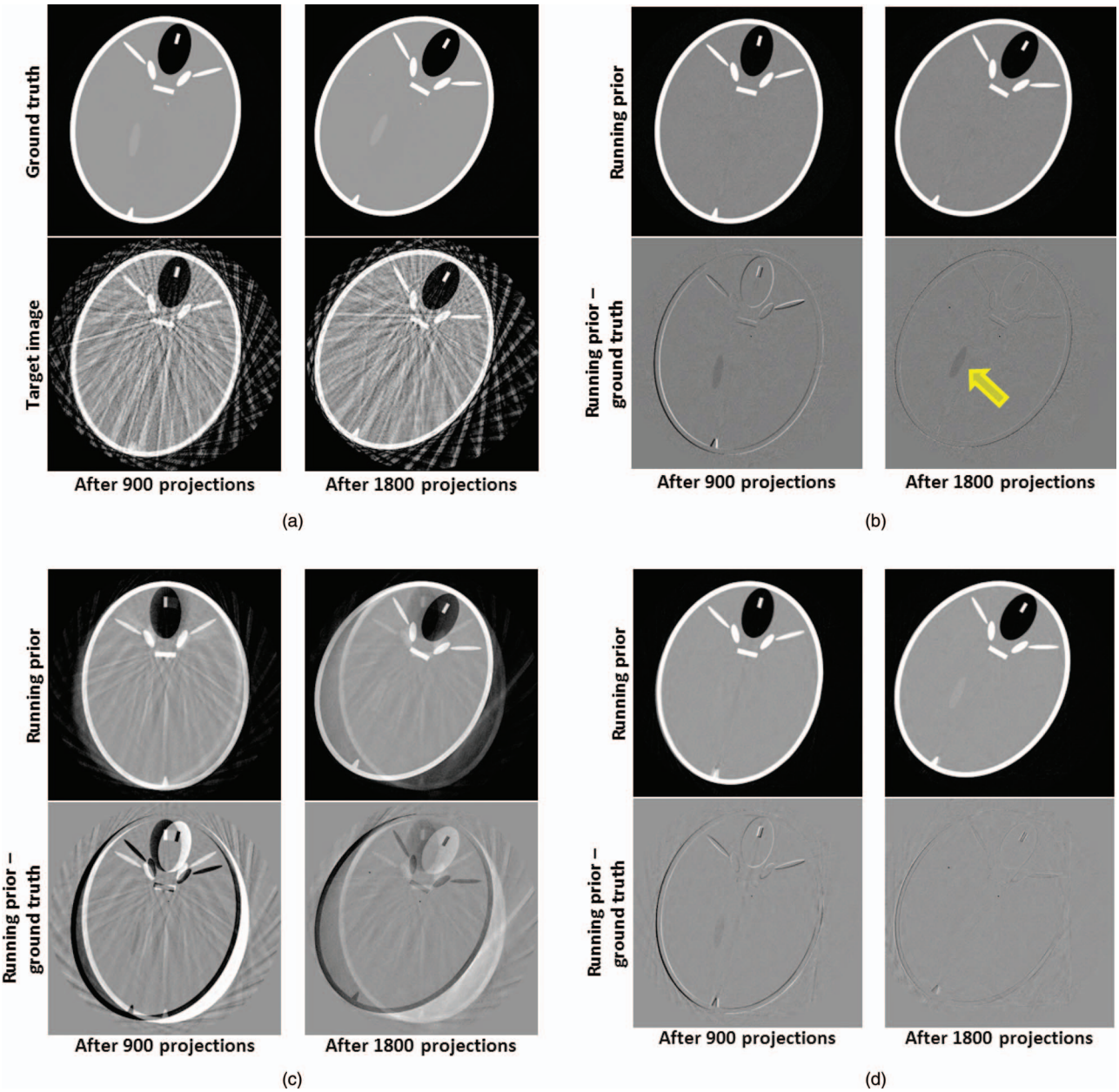

FIG. 10. Ground truth and running priors with and without registration or replacement. The left column of each subfigure is the situation around projection 900 while the right column represents images centered around projection 1800. The images are shown at a gray scale window $C = 0$ HU, $W = 2000$ HU. (a) Ground truth and target image; (b) running prior: registration, no replacement; (c) running prior: replacement, no registration; and (d) running prior: registration and replacement.

reconstructed on a 512 × 512 × 256 voxel grid with voxel size 0.5 mm × 0.5 mm × 0.5 mm.

2.E.1. Simulation

In our simulation 1800 projections were acquired. The first $N_P = 600$ projections belong to the prior scan and are calculated equiangularly distributed over a full rotation. The following 1200 projections are acquired within 40 rotations with an angular spacing of about 12° resulting in $N_I = 15$ projections per 180°. The head phantom was simulated. After 600 projections an ellipsoid with an attenuation of 150 HU was added to the phantom (see Fig. 6).

From projection 601 the phantom (including the ellipsoid) is translated continuously 20 mm in x-direction and rotated about 30° around the z-axis over the following 600 projections. For the last 600 projections, the phantom does not move anymore. The position of the phantom throughout the scan is illustrated in Fig. 7 together with a virtual time line corresponding to a real measurement. During the simulated intervention scan, from projection 601 to projection 1800, a guide wire which is simulated by small cylinders arranged on a spline is inserted into the phantom.

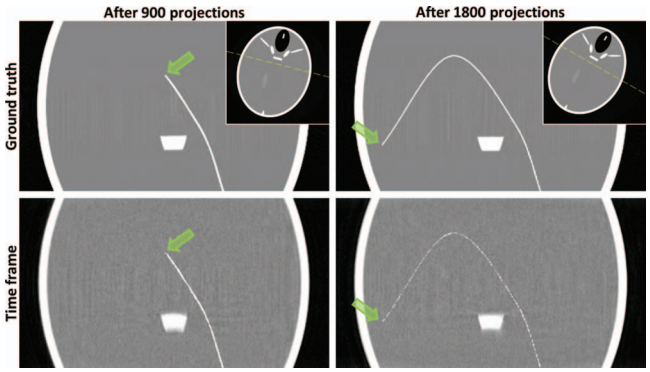

FIG. 11. Ground truth and time frames are shown to demonstrate that the position of the simulated guide wire can be reconstructed correctly using the running prior. The images are shown at a gray scale window $C = 0$ HU, $W = 2000$ HU.

Before reconstruction Poisson-distributed noise was added to the projections resulting in a standard deviation of 70 HU in water-equivalent tissue in the prior image.

2.E.2. Measurements

A prototype volume CT (Siemens Healthcare, Forchheim, Germany) was used for the measurements. This CT-system consists of a flat detector mounted into a clinical gantry. Using this system, it was possible to perform continuous rotation during the intervention scan. A pig was scanned *in vivo* while the carotid and the facial artery were probed with a guide wire inserted via a catheter. The experimental setup as well as the interventional materials used for the intervention are shown in Fig. 8. During the intervention the pig was anesthetized via an injection of a combination of 8 mg/kg body weight of azaperon, 1 mg/kg body weight of midazolam, and 20 mg/kg body weight of ketamine. While anesthetized the pig still breathed free. All animal experiments were approved by the governmental animal ethics committee (Regierungspräsidium Karlsruhe).

During the prior scan $N_P = 600$ projections were acquired within a single 20 s rotation. For the data of the intervention scan, a standard protocol with a sampling rate of 30 frames/s and a gantry rotation time of 4 s was applied. From these data only every fourth projection is used for reconstruction. That means only $N_I = 15$ projections, distributed over 180°, are used for the calculation of each time frame. Both scans are performed at 80 kV tube voltage and 50 mA tube current, but the intervention scan was pulsed resulting in a mean tube current of 18 mA.

To get a dataset with motion the pig was moved manually between prior and intervention scan like demonstrated in Fig. 9. In contrast to the simulation the motion of the pig is not only an affine transformation but a non-rigid deformation.

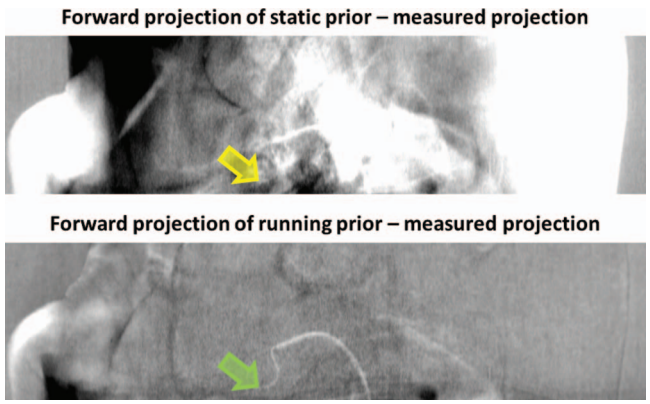

FIG. 12. Raw data difference: forward projected static or running prior minus the measured projections at an angle of 220°. The images are shown at a gray scale window $C = 0.0$, $W = 0.5$.

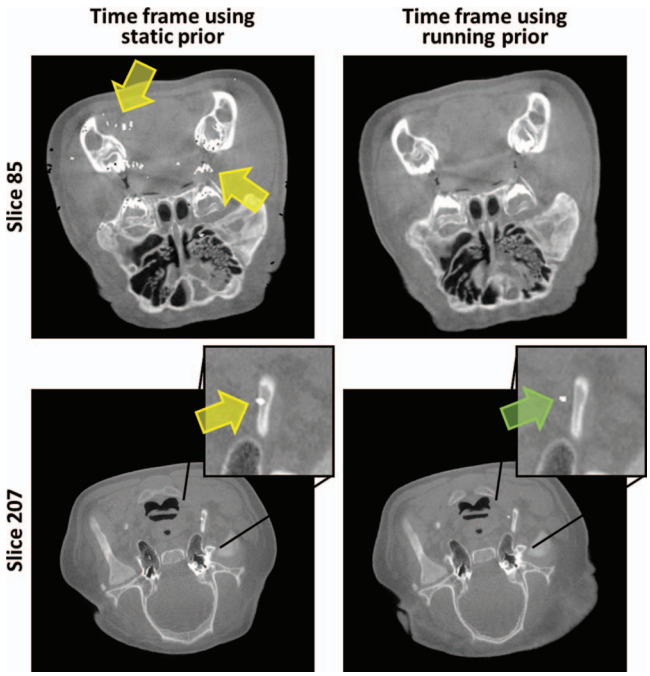

FIG. 13. Comparison of PrIDCIT time frames based on the static prior or the running prior. The images are shown at a gray scale window $C = 0$ HU, $W = 1500$ HU.

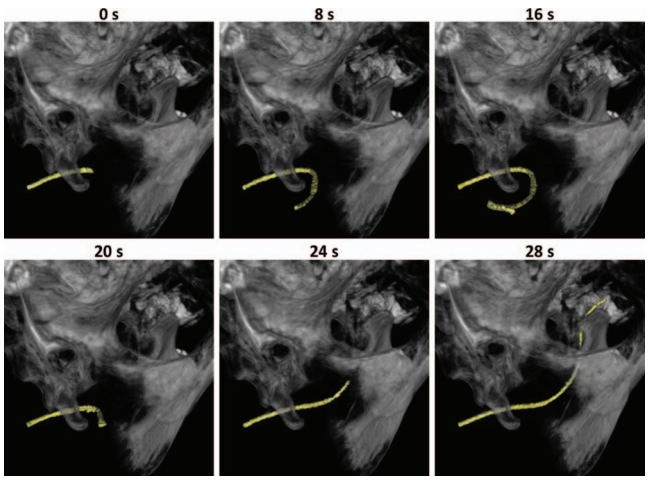

FIG. 14. Volume rendering of different time frames of a probing intervention. The pig moved between the prior and the intervention scan which requires the running prior for correct reconstruction.

3. RESULTS

3.A. Simulation

To show that both the registration and the projection replacement are necessary, we selectively switch on either step or both steps simultaneously (Fig. 10). The results with registration but without replacing information of older projections by newer projections can correct for motion while changes in soft tissue are not attended to [Fig. 10(b)] because the ellipsoid simulating an intracranial hematoma does not appear in the running prior.

If the replacement step without the registration is used, it is not possible to correct for motion [Fig. 10(c)], which is quite obvious. If motion stops, the running prior converges to the new situation but that would last longer than shown here. Apparently, the replacement step is somewhat less important than the registration step.

A combination of both steps, registration, and replacement, yields the desired results [Fig. 10(d)]. As can be seen the method can correct for motion as well as changes in the anatomy. In particular the ellipsoid, representing the intracranial hematoma, is well displayed in the running prior centered around projection 1800. It is not clearly visible at the running prior centered around projection 90 because the temporal resolution of soft tissue changes corresponds to $N_P = 600$ projections.

In intervention guidance, it is of highest importance to get an immediate visual feedback of the location of the interventional materials in relation to the surrounding anatomy. As can be seen from Fig. 11, which shows the simulated guide wire, this is well handled with PrIDICT based on the running prior. The position of the guide wire is the same as in the ground truth as indicated by the arrows which are at the same position in the ground truth and in the correspondent time frame. Because of the low number of noisy projections used for reconstructing the time frames the guide wire does not look as nice as in the ground truth. But that is not the problem in intervention guidance. The focus here is on the recognition of the guide wire and especially the tip as well as a high temporal resolution. The temporal resolution of the interventional materials corresponds to $N_I = 15$ projections or a half rotation which is much higher than the temporal resolution of soft tissue changes.

3.B. Measurements

We use the *in vivo* measurements to demonstrate and evaluate the running prior technique in a clinical setup where nonrigid motion occurs and other physical effects impair the quality of the data. As we had seen in Fig. 9, the registration with the demons algorithm leads to a high correlation between the running prior and the target image. To follow up, Fig. 12 regards the difference between forward projections of the static or the running prior and measured projection data. With the prior well chosen it is to expect that the difference image shows only the interventional materials which is a guide wire inserted into the vasculature through a catheter in this case. In other words, this difference image should be sparse. Regarding Fig. 12, we find that the raw data difference using the static prior is not sparse because of motion while the raw data difference using our new running prior is sparse and it shows the guide wire and its tip very well. Consequently, only the running prior is suitable to apply the PrIDICT algorithm.

Figure 13 shows the corresponding time frames. Obviously those images based on the static prior are significantly affected by motion artifacts which generate spurious white or black pixels in the PrIDICT algorithm (arrows in the top row). Even worse, the interventional material is displayed at a wrong position in relation to the patient's anatomy. For example, in the lower row of Fig. 13 the guide wire is running through the mandible (arrows) which is physically impossible because the guide wire is inserted into the vasculature and not into bone.

With the running prior the time frames show the true relationship between the guide wire and the surrounding anatomy. The guide wire is displayed at the correct position and the images contain significantly less artifacts.

In addition some time frames of the resulting 4D volume are provided as volume rendering, created with the software ImageVis3D,[16] in Fig. 14. This figure emphasizes the three-dimensional nature of the approach and may give an idea of what could, potentially, be displayed during intervention.

4. CONCLUSION AND DISCUSSION

We proposed a method to continuously adapt prior knowledge to the current situation in an image-guided intervention. This adaptation consists of a registration of the prior combined with a replacement of outdated projections. Simulated data and an animal *in vivo* study showed that our approach significantly improves the timeliness of the prior information. In particular neither the registration nor the replacement step should be used alone because only their combination promises images of sufficient quality.

It is not possible to display the correct position of interventional materials without the running prior when the patient moves between prior and intervention scan. Furthermore, the volumes reconstructed by PrIDICT using a static prior in case of motion are deteriorated by artifacts. Only when using the running prior technique the interventional materials are displayed at the correct position in time frames of high image quality without artifacts. The running prior works in case of motion between prior and intervention scan (see Sec. 3.B), it works in case of motion during the intervention itself (see Sec. 3.A) and, obviously, it works in case of no motion because then it reduces to the static prior.

For a clinical application, it is required that the running prior is calculated in real-time. Our current calculation times are in the range of some minutes performed on a 64 bit version of Windows 7 system equipped with two Intel Xeon X5690 processors. But the very intent of this study was to show that it is feasible to adapt the prior without additional dose. So we do not focus on optimizing our source code for speed. In addition

parallelization and future developments regarding computer power would make a real-time computation possible.

So far tomographic fluoroscopy at a dose level comparable to the projective fluoroscopy was demonstrated only in experimental settings without patient motion corresponding best with neuro-interventional procedures where the patient's head can be fixated to ensure no motion during the intervention. Of course in tomographic fluoroscopy the dose for acquiring a prior image has to be taken into account. Given that in many interventions today one or more 3D volumes are acquired in-between phases of projective fluoroscopy, this implies similar or even higher dose levels than for our proposed method. In consequence, the tomographic fluoroscopy may become an alternative to single- or biplane fluoroscopy also in other fields of interventional radiology besides neuro-interventional procedures.

While we were only able to test simple motion patterns in our study, quasi periodic motion, such as respiratory or cardiac motion, is occurring in many interventional situations too. For example, the transcatheter aortic valve implantation (TAVI) procedure will suffer from such cyclic motion. In those cases, we anticipate that the running prior will need additional adaptation because in its current version it is not capable of capturing such high motion frequencies. Probably such an extension would require to determine the typical motion components from the prior scan, and to integrate those into the running prior.

It should be noted that the running prior technique is not restricted to be used with the PrIDICT algorithm. Potentially, the running prior concept can be combined with and be useful for other types of algorithms or even other applications.

We conclude that the running prior technique is one important step toward robust tomographic fluoroscopy at dose levels as low as in projective fluoroscopy. However, no system apart from our experimental setup is able to provide such low dose tomographic fluoroscopy images yet. Today one may only speculate about the impact of such a new image guidance modality which would allow to move intervention guidance from 2D projective images to 3D tomographic images, and thereby allow for completely new minimally invasive interventions.

ACKNOWLEDGMENTS

This study was supported by the Deutsche Forschungsgemeinschaft (DFG) under Grant No. KA 1678/6-1. The high performance compute hardware was provided by the Universitätsbund Erlangen-Nürnberg e.V., Erlangen, Germany. Parts of the reconstruction software were provided by RayConStruct® GmbH, Nürnberg, Germany.

[a]Author to whom correspondence should be addressed. Electronic mail: barbara.flach@dkfz.de; Telephone: +49 (6221) 42 3068; Fax.: +49 (6221) 42 2585.

[1]A. Brill, J. Fleshman, Jr., B. Ramshaw, S. Wexner, and O. Kaidar-Person, "Minimally invasive procedures: What family physicians need to know," J. Fam. Pract. (Suppl.), S1–S22 (2005).

[2]K. Cleary and T. Peters, "Image-guided interventions: Technology review and clinical applications," Annu. Rev. Biomed. Eng. **12**, 119–142 (2010).

[3]UNSCEAR (United Nations Scientific Committee on the Effects of Atomic Radiation), *Sources and Effects of Ionizing Radiation, UNSCEAR 2008 Report: Volume I: Sources — Report to the General Assembly Scientific Annexes A and B* (United Nations University Press, NY, 2010).

[4]National Council on Radiation Protection and Measurements, "Radiation dose management for fluoroscopically guided interventional medical procedures," NCRP Report No. 168 (NCRP, Bethesda, MD, 2010).

[5]IAEA, "Patient dose optimization in fluoroscopically guided interventional procedures," Technical Document Series No. 1641 (International Atomic Energy Agency, Vienna, 2010).

[6]E. Paulson, D. Sheafor, D. Enterline, H. McAdams, and T. Yoshizumi, "CT fluoroscopy–guided interventional procedures: Techniques and radiation dose to radiologists," Radiology **220**, 161–167 (2001).

[7]R. Silbergleit, B. Mehta, W. Sanders, and S. Talati, "Imaging-guided injection techniques with fluoroscopy and CT for spinal pain management," Radiographics **21**, 927–939 (2001).

[8]A. Wagner, "CT fluoroscopy–guided epidural injections: Technique and results," Am. J. Neuroradiol. **26**, 1821–1823 (2004).

[9]R. Nawfel, P. Judy, S. Silverman, S. Hooton, K. Tuncall, and D. Adams, "Patient and personnel exposure during CT fluoroscopy-guided interventional procedures," Radiology **216**, 180–184 (2000).

[10]N. Keat, "Real-time CT and CT fluoroscopy," Br. J. Radiol. **74**, 1088–1090 (2001).

[11]S. Carlson, C. Bender, K. Classic, F. Zink, J. Quam, E. Ward, and A. Oberg, "Benefits and safety of CT fluoroscopy in interventional radiologic procedures," Radiology **219**, 515–520 (2001).

[12]B. Daly and P. Templeton, "Real-time CT fluoroscopy: Evolution of an interventional tool," Radiology **211**, 309–315 (1999).

[13]J. de Mey, B. Op de Beeck, M. Meysman, M. Noppen, M. De Maeseneer, M. Vanhoey, W. Vincken, and M. Osteaux, "Real time CT-fluoroscopy: Diagnostic and therapeutic applications," Eur. J. Radiol. **34**, 32–40 (2000).

[14]J. Kuntz, R. Gupta, S. Schönberg, W. Semmler, M. Kachelrieß, and S. Bartling, "Real-time X-ray-based 4D image guidance of minimally invasive interventions," Eur. Radiol. **23**, 1669–1677 (2013).

[15]J. Kuntz, B. Flach, R. Kueres, W. Semmler, M. Kachelrieß, and S. Bartling, "Constrained reconstructions for 4D intervention guidance," Phys. Med. Biol. **58**, 3283–3300 (2013).

[16]T. Fogal and J. Krüger, "Tuvok, an architecture for large scale volume rendering," in *Proceedings of the 15th International Workshop on Vision, Modeling, and Visualization* (Eurographics, 2010).

[17]E. Sidky, C. Kao, and X. Pan, "Accurate image reconstruction from few-views and limited-angle data in divergent-beam CT," J. X-Ray Sci. Technol. **14**, 119–139 (2006).

[18]L. Ritschl, F. Bergner, C. Fleischmann, and M. Kachelrieß, "Improved total variation-based CT image reconstruction applied to clinical data," Phys. Med. Biol. **56**, 1545–1561 (2011).

[19]G. Chen, J. Tang, and S. Leng, "Prior image constrained compressed sensing (PICCS): A method to accurately reconstruct dynamic CT images from highly undersampled projection data sets," Med. Phys. **35**, 660–663 (2008).

[20]J. Lee, J. Stayman, Y. Otake, S. Schafer, W. Zbijewski, A. Khanna, J. Prince, and J. Siewerdsen, "Volume-of-change cone-beam CT for image-guided surgery," Phys. Med. Biol. **57**, 4969–4989 (2012).

[21]S. Balter, J. Hopewell, D. Miller, L. Wagner, and M. Zelefsky, "Fluoroscopically guided interventional procedures: A review of radiation effects on patients' skin and hair," Radiology **254**, 326–341 (2010).

[22]A. Norbash, D. Busick, and M. Marks, "Techniques for reducing interventional neuroradiologic skin dose: Tube position rotation and supplemental beam filtration," Am. J. Neuroradiol. **17**, 41–49 (1996).

[23]F. Hentschel, I. Habermaas, S. Bien, and W. Seeger, "Abschätzung der Strahlenbelastung bei interventionellen neuroradiologischen Eingriffen am Kopf von Kindern im Vergleich zur Exposition erwachsener Patienten," RöFo **165**, 176–180 (1996).

[24]N. Gkanatsios, W. Huda, K. Peters, and J. Freeman, "Evaluation of an online patient exposure meter in neuroradiology," Radiology **203**, 837–842 (1997).

[25]International Commission on Radiation Protection, "Avoidance of radiation injuries from medical interventional procedures," Ann. ICRP **85**, 7–51 (2000).

[26]M. Mahesh, "Fluoroscopy: Patient radiation exposure issues," Radiographics **21**, 1033–1045 (2001).

[27]G. Kemerink, M. Frantzen, K. Oei, M. Sluzewski, W. van Rooij, J. Wilmink, and J. van Engelshoven, "Patient and occupational dose in neurointerventional procedures," Interv. Neuroradiol. **44**, 522–528 (2002).
[28]D. Miller, S. Balter, P. Cole, H. Lu, B. Schueler, M. Geisinger, A. Berenstein, R. Albert, J. Georgia, P. Noonan, J. Cardella, J. St. George, E. Rusell, T. Malisch, and R. Vogelzang, "Radiation doses in interventional radiology procedures: The RAD-IR study: Part I: Overall measures of dose," J. Intervasc. Radiol. **14**, 711–727 (2003).
[29]J. Winston, K. Best, L. Plusquellic, and P. Thoma, *Patient Exposure and Dose Guide — 2003* (CRCPD, Frankfort, KY, 2003).
[30]H. Iida, J. Horii, M. Chabatake, E. Taka, M. Shimizu, and T. Mizushima, "Evaluation and estimation of entrance skin dose in patients undergoing diagnostic and interventional radiology procedures," Nihon Hoshasen Gijutsu Gakkai Zasshi **60**, 126–135 (2004).
[31]N. Swoboda, D. Armstrong, J. Smith, E. Charkot, and B. Connolly, "Pediatric patient surface doses in neuroangiography," Pediatr. Radiol. **35**, 859–866 (2005).
[32]H. Geijer, T. Larzon, R. Popek, and K. Beckman, "Radiation exposure in stent-grafting of abdominal aortic aneurysms," Br. J. Radiol. **78**, 906–912 (2005).
[33]D. Bor, S. Cekirge, T. Türkay, O. Turan, M. Gülay, E. Onal, and B. Cil, "Patient and staff doses in interventional neuroradiology," Radiat. Prot. Dosim. **117**, 62–68 (2005).
[34]R. Ukisu, T. Kushihashi, and I. Soh, "Skin injuries caused by fluoroscopically guided interventional procedures: Case-based review and self-assessment module," Am J. Roentgenol. **193**, S59–S69 (2009).
[35]M. Alexander, M. Oliff, O. Olorunsola, M. Brus-Ramer, E. Nickoloff, and P. Meyers, "Patient radiation exposure during diagnostic and therapeutic interventional neuroradiology procedures," J. Neurointerv. Surg. **2**, 6–10 (2010).
[36]K. Chida, M. Kato, Y. Kagaya, M. Zuguchi, H. Saito, T. Ishibashi, S. Takahashi, S. Yamada, and Y. Takai, "Radiation dose and radiation protection for patients and physicians during interventional procedure," J. Radiat. Res. (Tokyo) **51**, 97–105 (2010).
[37]J. Urairat, S. Asavaphatiboon, S. Singhara Na Ayuthaya, and N. Pongnapang, "Evaluation of radiation dose to patients undergoing interventional radiology procedures at Ramathibodi Hospital, Thailand," Biomed. Imaging Interv. J. **7**, e22 (2011).
[38]International Atomic Energy Agency (IAEA), *Fluoroscopy* (IAEA, Vienna, Austria, 2013), https://rpop.iaea.org/RPOP/RPoP/Content/InformationFor/HealthProfessionals/1_Radiology/Fluoroscopy.htm.
[39]R. Anxionnat, S. Bracard, X. Ducrocq, Y. Trousset, L. Launay, E. Kerrien, M. Braun, R. Vaillant, F. Scomazzoni, A. Lebedinsky, and L. Picard, "Intracranial aneurysms: Clinical value of 3D digital subtraction angiography in the therapeutic decision and endovascular treatment," Radiology **218**, 799–808 (2001).
[40]T. Abe, M. Hirohata, N. Tanaka, Y. Uchiyama, K. Kojima, K. Fujimoto, A. Norbash, and N. Hayabuchi, "Clinical benefits of rotational 3d angiography in endovascular treatment of ruptured cerebral aneurysm," Am. J. Neuroradiol. **23**, 686–688 (2002).
[41]G. Richter, T. Engelhorn, T. Struffert, M. Doelken, O. Ganslandt, J. Hornegger, W. Kalender, and A. Doerfler, "Flat panel detector angiographic CT for stent-assisted coil embolization of broad-based cerebral aneurysms," Am. J. Neuroradiol. **28**, 1902–1908 (2007).
[42]K. Namba, Y. Niimi, J. Song, and A. Berenstein, "Use of Dyna–CT angiography in neuroendovascular decision-making: A case report," Interv. Neuroradiol. **15**, 67–72 (2009).
[43]L. Feldkamp, L. Davis, and J. Kress, "Practical cone-beam algorithm," J. Opt. Soc. Am. **1**, 612–619 (1984).
[44]B. Flach, J. Kuntz, M. Brehm, S. Bartling, and M. Kachelrieß, "Running prior for patient motion correction in low-dose 3D+time interventional flat detector CT," in *2012 IEEE Nuclear Science Symposium and Medical Imaging Conference (NSS/MIC)* (IEEE, Anaheim, CA, 2012), pp. 2395–2401.
[45]P. Viola and W. Wells, "Alignment by maximization of mutual information," Int. J. Comput. Vis. **24**, 137–154 (1997).
[46]F. Herrera and M. Lozano, "Two-loop real-coded genetic algorithms with adaptive control of mutation step sizes," Appl. Intell. **13**, 187–204 (2000).
[47]J. Thirion, "Image matching as a diffusion process: An analogy with Maxwell's demons," Med. Image Anal. **2**, 243–260 (1998).
[48]See www.itk.org.